Treating geometric phase effects in nonadiabatic dynamics

Alex Krotz and Roel Tempelaar[*]

Department of Chemistry, Northwestern University, 2145 Sheridan Road, Evanston, Illinois 60208, USA

We present an approach for eliminating the gauge freedom for derivative couplings, enabling nonadiabatic dynamics in the presence of geometric phase effects. This approach relies on a bottom-up construction of a parametric quantum Hamiltonian in terms of functions of a dynamical variable. These functions can be associated with real- and imaginary-valued contributions to the Hamiltonian in a given diabatic basis. By minimizing variable-dependent fluctuations of the imaginary functions we identify a set of diabatic bases that recover the real-valued gauge commonly used for topologically trivial systems. This minimization, however, also confines the gauge freedom in the topologically nontrivial case, opening a path towards finding gauge-invariant derivative couplings under geometric phase effects. Encouraging results are presented for fewest-switches surface-hopping calculations of a nuclear wave packet traversing an avoided-crossing region, for which fully gauge-invariant derivative couplings are found.

I. INTRODUCTION

It is well known that the parametric dependence of a quantum Hamiltonian on a dynamical variable may give rise to geometric phase effects that influence the dynamics [1–3]. This is particularly relevant to mixed quantum-classical dynamics which involves a quantum Hamiltonian that depends parametrically on classical coordinates [4,5]. In topologically trivial systems the nonadiabatic rotation of the quantum eigenbasis induced by the classical coordinates is captured by the derivative couplings between eigenstates which can be made real valued by appropriately adjusting the gauge of the eigenbasis [6]. In topologically nontrivial systems, however, the derivative coupling also captures a "geometric" rotation that is orthogonal to the otherwise real-valued nonadiabatic rotation.

In addition to imposing a path-dependent phase on individual eigenstates in the adiabatic limit [1], the geometric rotation introduces a complex contribution to the derivative couplings between eigenstates [7]. As a result, the derivative couplings can no longer be made real valued by a gauge transformation. This complicates the description of topologically nontrivial systems by trajectory surface hopping techniques [8–11], such as the widely used fewest-switches surface-hopping (FSSH) method [12,13], where real-valued vectors associated with derivative couplings are required to determine the direction in which to rescale classical momenta upon nonadiabatic transitions (hops). Recent years have seen growing interest in the application of trajectory surface hopping to problems featuring nontrivial topologies [14–18], including pronounced spin-dependent behavior [19–24], conical intersections [25–27], intersystem crossings [28–30], and Dirac cones [31–33], prompting investigations into the influence of

geometric phase effects within this class of techniques and on the momentum rescaling directions in particular [34–36].

Traditionally, momentum rescaling directions have been associated with the instantaneous limit of the Pechukas force arising from a nonadiabatic transition [35,37,38]. In this limit, the Pechukas force becomes an impulsive one in the direction of the real part of the derivative coupling and so is real valued by construction [9]. Nevertheless, the direction of the real part of the derivative coupling is generally not gauge invariant. Indeed, even in the topologically trivial case, a gauge exists where the derivative coupling becomes fully imaginary, as a result of which the direction of its real part becomes undefined [39].

If anything, this suggests that previous works have adopted an implicit gauge fixing which at the very least disfavors this "singular gauge." An obvious choice of gauge for the topologically trivial case is then one in which the derivative couplings become fully real valued, consistent with the traditional application of trajectory surface hopping techniques to systems with real-valued eigenvectors. In the topologically nontrivial case, however, there is no gauge in which the derivative couplings become fully real valued, and a change in gauge rotates their real part, changing the momentum rescaling directions. The sudden appearance of a gauge ambiguity when geometric phase effects are introduced motivates the formulation of a more general treatment that applies to both the topologically trivial and nontrivial cases, necessarily recovering real-valued derivative couplings in the former and restricting the gauge freedom in the latter.

In this article we pursue this goal by presenting a bottom-up construction of a parametric quantum Hamiltonian in terms of functions of a dynamical variable. These functions can be associated with real- and imaginary-valued contributions to the Hamiltonian in a given diabatic basis. We then recognize that in certain "preferred" bases the functions associated with the imaginary-valued contributions can be taken as *constants*

* roel.tempelaar@northwestern.edu

in the topologically trivial case, consequently giving rise to strictly real-valued derivative couplings. This allows us to employ the *fluctuations* of these functions as a metric which can be minimized to yield real-valued derivative couplings, thereby resolving the singular-gauge ambiguity.

By employing the aforementioned metric we establish a continuity between the topologically trivial and nontrivial cases, enabling us to radically restrict the gauge freedom for complex-valued derivative couplings arising in the topologically nontrivial case, thereby reducing the ambiguity in the direction of their real parts. Moreover, for a series of two-dimensional avoided-crossing problems we show empirically that this approach yields fully gauge-invariant momentum rescaling directions, while its implementation within FSSH yields encouraging results when compared to exact quantum modeling. In addition to shedding light on the fundamental properties of derivative couplings, our theory guides the gauge-invariant implementation of trajectory surface hopping techniques in the presence of geometric phase effects and provides a path towards incorporating such effects in future mixed quantum-classical dynamics methods.

II. THEORY

We begin by considering an arbitrary quantum Hamiltonian that depends parametrically on a classical coordinate $\boldsymbol{q}$. This Hamiltonian can be represented by a set of real-valued scalar functions of $\boldsymbol{q}$, an obvious choice for which are the real and imaginary parts of the Hamiltonian matrix elements. Assuming the Hamiltonian is N-dimensional and traceless, we need at most $N^2 - 1$ functions to define it and can discard at least $N' = \frac{1}{2}(N^2 - N)$ functions if the Hamiltonian is constrained to be topologically trivial with real-valued matrix elements.

Naturally, these functions depend on the diabatic basis used to express the Hamiltonian. For example, a topologically trivial Hamiltonian that has real-valued matrix elements in one diabatic basis may have complex-valued matrix elements in another. Importantly, this may give rise to complex-valued eigenvectors and, consequently, complex-valued derivative couplings [40], which implies that the applied functional representation still captures some of the gauge freedom of the derivative couplings, including the singular gauge. However, as shown below, by imposing that topologically trivial Hamiltonians necessarily give rise to real-valued derivative couplings, we can directly use the functions to avoid the singular gauge.

To this end we must assess the eigenvector matrix in terms of the functions. This can be achieved by analytic diagonalization of the Hamiltonian, but doing so becomes intractable in higher dimensions. Instead, we utilize the functions to directly construct a unitary matrix of column eigenvectors and a real-valued, traceless, and diagonal matrix of eigenvalues, both of which depend parametrically on $\boldsymbol{q}$ (after which the Hamiltonian can be obtained through the eigendecomposition).

A natural way to construct this representation is by using the generators of the group SU(N), which forms a basis of N-dimensional, traceless, anti-Hermitian matrices. While the particular form of each generator is arbitrary, we broadly classify them into three subsets: $\{T_{n_e}^E\}$, the subset of $N - 1$ imaginary-valued diagonal generators, $\{T_{n_r}^R\}$, the subset of

N' real-valued off-diagonal generators, and $\{T_{n_i}^I\}$, the subset of N' imaginary-valued off-diagonal generators. To formulate a generic traceless eigenvalue matrix we associate each imaginary-valued diagonal generator in $\{T_{n_e}^E\}$ with an "energetic" function of $\boldsymbol{q}$, λ_{n_e}, which linearly combines the generators to produce

$$E(\boldsymbol{\lambda}) = i \sum_{n_e} \lambda_{n_e} T_{n_e}^E. \tag{1}$$

The space of all possible traceless eigenvalue matrices is spanned through Eq. (1) by variations in the functions λ_{n_e}. If a given Hamiltonian H_0 has the eigendecomposition $H_0(\boldsymbol{q}) = V_0(\boldsymbol{q})E_0(\boldsymbol{q})V_0^\dagger(\boldsymbol{q})$, where E_0 and V_0 are its eigenvalue and eigenvector matrices, respectively, then $\boldsymbol{\lambda} = (\lambda_1, \lambda_2, \ldots, \lambda_{N-1})$ are its energetic functions if $E(\boldsymbol{\lambda}(\boldsymbol{q})) = E_0(\boldsymbol{q})$ is satisfied.

Next, we recognize that a given eigenvector matrix V_0 is associated with a subset of SU(N), the elements of which are related to one another by a gauge transformation. Accordingly, we can formulate a generic eigenvector matrix up to a gauge transformation as (see Appendix A for details)

$$V(\boldsymbol{I}, \boldsymbol{R}) = \prod_{n_i} \exp\left(I_{n_i} T_{n_i}^I\right) \prod_{n_r} \exp\left(R_{n_r} T_{n_r}^R\right) \equiv U(\boldsymbol{I})\tilde{V}(\boldsymbol{R}), \tag{2}$$

where $\boldsymbol{I} = (I_1, I_2, \ldots, I_{N'})$ are functions associated with the imaginary-valued off-diagonal generators and $\boldsymbol{R} = (R_1, R_2, \ldots, R_{N'})$ are functions associated with the real-valued off-diagonal generators. We take the ordering and choice of generators to be fixed as a convention.

A generic traceless Hamiltonian matrix then follows from the eigendecomposition as

$$H(\boldsymbol{\lambda}, \boldsymbol{I}, \boldsymbol{R}) = V(\boldsymbol{I}, \boldsymbol{R})E(\boldsymbol{\lambda})V^\dagger(\boldsymbol{I}, \boldsymbol{R}), \tag{3}$$

which, as expected, involves $N^2 - 1$ independent functions. If we discard U from the construction of V [Eq. (2)], by setting $\boldsymbol{I} = 0$, we can write a generic real-valued Hamiltonian as $\tilde{H}(\boldsymbol{\lambda}, \boldsymbol{R}) = \tilde{V}(\boldsymbol{R})E(\boldsymbol{\lambda})\tilde{V}^\dagger(\boldsymbol{R})$, which requires N' fewer functions. To represent a given traceless Hamiltonian H_0 using Eq. (3), one simply solves the equation $H(\boldsymbol{\lambda}(\boldsymbol{q}), \boldsymbol{I}(\boldsymbol{q}), \boldsymbol{R}(\boldsymbol{q})) = H_0(\boldsymbol{q})$, yielding a functional representation of H_0.

Once a Hamiltonian has been represented in terms of functions, these functions can be used to evaluate the derivative couplings, which follow from Eq. (2) as

$$\begin{aligned} V^\dagger(\boldsymbol{I}, \boldsymbol{R})\nabla V(\boldsymbol{I}, \boldsymbol{R}) &= \tilde{V}^\dagger(\boldsymbol{R})U^\dagger(\boldsymbol{I})\nabla U(\boldsymbol{I})\tilde{V}(\boldsymbol{R}) \\ &\quad + \tilde{V}^\dagger(\boldsymbol{R})\nabla\tilde{V}(\boldsymbol{R}), \end{aligned} \tag{4}$$

where ∇ denotes differentiation with respect to $\boldsymbol{q}$ and acts only on its adjacent term. Here, the term $\tilde{V}^\dagger(\boldsymbol{R})U^\dagger(\boldsymbol{I})\nabla U(\boldsymbol{I})\tilde{V}(\boldsymbol{R})$ is generally complex valued and vanishes when $\boldsymbol{I} = 0$. It therefore does not contribute to the derivative coupling when the Hamiltonian is topologically trivial and real valued. More generally, it does not contribute when $\nabla \boldsymbol{I} = 0$, i.e., in the absence of fluctuations of $\boldsymbol{I}$ with $\boldsymbol{q}$ [41]. Indeed, for topologically trivial Hamiltonians with $\nabla \boldsymbol{I} = 0$ the nonadiabatic rotation of the eigenbasis is entirely captured by $\tilde{V}^\dagger(\boldsymbol{R})\nabla\tilde{V}(\boldsymbol{R})$, which is real valued by construction. As a result, it is appropriate to use this term to determine momentum rescaling directions.

However, as previously mentioned, a topologically trivial Hamiltonian can be made complex valued by a diabatic basis transformation, as a result of which $\nabla I \neq 0$ and $\tilde{V}^\dagger(\boldsymbol{R})\nabla\tilde{V}(\boldsymbol{R})$ no longer exclusively incorporates the nonadiabatic rotation. Importantly, however, in such cases, one can always find a diabatic basis for which $\nabla I = 0$. This basis is part of a set of "preferred bases" for which $\tilde{V}^\dagger(\boldsymbol{R})\nabla\tilde{V}(\boldsymbol{R})$ optimally captures the nonadiabatic rotation. Hence, in practice one may solve $H(\lambda(\boldsymbol{q}), I^k(\boldsymbol{q}), \boldsymbol{R}^k(\boldsymbol{q})) = D_k^\dagger H_0(\boldsymbol{q}) D_k$ for arbitrary diabatic transformations D_k, where $\boldsymbol{R}^k$, I^k, and λ are the functions representing the Hamiltonian associated with D_k, while minimizing fluctuations of I^k. (We note that λ is independent of the diabatic basis and therefore does not carry a k dependence.)

For simplicity, consider the case where I^k consists of only a single function I^k which depends on a one-dimensional coordinate q. Fluctuations of I^k can be assessed in terms of its Taylor series as

$$I^k(q+\epsilon) - I^k(q) = \sum_{m=1}^{\infty} \frac{1}{m!} \frac{\partial^m I^k(q)}{\partial q^m} \epsilon^m, \qquad (5)$$

which for any constant I^k is exactly zero for any displacement ϵ. By taking I^k to be a vector in the mononomial basis in orders of ϵ, the coefficients in Eq. (5) can be considered elements of the vector describing the displacement of I^k from the point of constancy, defined by the zeroth-order element which is subtracted out in Eq. (5). The Euclidean distance of I^k from this point,

$$\text{dist}[I^k(q)] = \sqrt{\sum_{m=1}^{\infty} \left(\frac{1}{m!} \frac{\partial^m I^k(q)}{\partial q^m} \epsilon^m \right)^2}, \qquad (6)$$

then provides a metric for the extent to which I^k is locally constant for a given value of ϵ.

A global metric can then be obtained by integrating Eq. (6) over q,

$$\mathfrak{D}(I^k) = \Omega^{-1} \int \text{dist}[I^k(q)] \, dq, \qquad (7)$$

and normalizing by the area integrated Ω. For multidimensional coordinates $\boldsymbol{q}$, Eq. (6) is trivially generalized to include the terms of the multidimensional Taylor series, and for multiple functions $\boldsymbol{I}^k = (I_1^k, I_2^k, \ldots, I_{N'}^k)$ the individual contributions to the distance can be directly summed.

Solving $H(\lambda(\boldsymbol{q}), \boldsymbol{I}^k(\boldsymbol{q}), \boldsymbol{R}^k(\boldsymbol{q})) = D_k^\dagger H_0(\boldsymbol{q}) D_k$ while minimizing $\mathfrak{D}(\boldsymbol{I}^k)$ across diabatic bases for arbitrarily large ϵ not only recovers fully real-valued derivative couplings for the topologically trivial case but also provides a means for extending the concept of preferred bases to topologically nontrivial Hamiltonians. While there is no diabatic basis in which a topologically nontrivial Hamiltonian has $\nabla \boldsymbol{I}(\boldsymbol{q}) = 0$, taking the preferred bases to be those which minimize $\mathfrak{D}(\boldsymbol{I}^k)$ provides an extension which continuously reduces to the topologically trivial case. This therefore offers a consistent framework for decomposing the derivative couplings through Eq. (4). The purely real contribution, $\tilde{V}^\dagger(\boldsymbol{R})\nabla\tilde{V}(\boldsymbol{R})$, then serves to determine the momentum rescaling directions.

Specifically for the $N = 2$ case, an arbitrary traceless Hamiltonian in some given diabatic basis takes the form

$$H_0(\boldsymbol{q}) = \rho(\boldsymbol{q}) \begin{pmatrix} -\cos\theta(\boldsymbol{q}) & \sin\theta(\boldsymbol{q})e^{i\phi(\boldsymbol{q})} \\ \sin\theta(\boldsymbol{q})e^{-i\phi(\boldsymbol{q})} & \cos\theta(\boldsymbol{q}) \end{pmatrix}, \qquad (8)$$

which involves only a single generator for each of the three subsets and hence a single function for each. Evaluating $\mathfrak{D}(I^k)$ for the solutions of $H(\lambda(\boldsymbol{q}), I^k(\boldsymbol{q}), R^k(\boldsymbol{q})) = D_k^\dagger H_0(\boldsymbol{q}) D_k$ enables one to find the set of preferred bases in which this metric is minimized. We demonstrate the construction of H according to Eq. (3) in Appendix B.

III. RESULTS

We now proceed with an application of our approach, which we henceforth refer to as $\mathfrak{D}_{\min}$, to three models involving a nuclear wave packet traversing an avoided-crossing region, governed by Eq. (8) under different parametrizations. For the resulting two-dimensional Hamiltonians, the functions can be found analytically, upon which the metric and momentum rescaling directions can be computed throughout all possible diabatic bases. In the Supplemental Material (SM) [42], we present such a survey for all of the models under the various applied parameter values. The accuracy of the computed rescalings is then assessed within FSSH. A comprehensive review of the application of FSSH to topologically trivial systems can be found elsewhere [12,13]. For topologically nontrivial systems, the contribution of the diagonal elements of the derivative coupling to the classical momentum gives rise to a "pseudomagnetic" gauge field which yields an additional force in the classical equations of motion. A detailed derivation of these equations of motion can be found in Appendix C.

A. Model A

In the first model, referred to as model A, Eq. (8) is parameterized as

$$\rho = A, \quad \theta = \frac{\pi}{2}[\text{erf}(Bx) + 1], \quad \phi = Wy, \qquad (9)$$

where we take $\boldsymbol{q} = (x, y)$. The resulting Hamiltonian is real valued when $W = 0.0$, corresponding to the topologically trivial case, and becomes increasingly nontrivial for larger values of W. Shown in Fig. 1 are the associated diabatic and adiabatic surfaces, where it can be seen that adiabatic surfaces are at a constant energy of $\pm A$, while the diabatic surfaces involve a single crossing at $x = 0$. Away from this crossing region, both surfaces converge on one another. Also depicted in Fig. 1 is $\sin\phi$, whose fluctuations are indicative of the complex phase of the eigenvectors due to geometric phase effects.

This model was previously investigated in detail in Ref. [35], where FSSH was applied while determining momentum rescaling directions based on whichever gauge maximized the real part of the derivative coupling at that point in the trajectory. This approach, which we refer to as $\mathfrak{R}_{\max}$, yielded promising results for some values of B and W. However, it induces abrupt changes in the momentum rescaling (between the x and y directions) when the magnitude of the
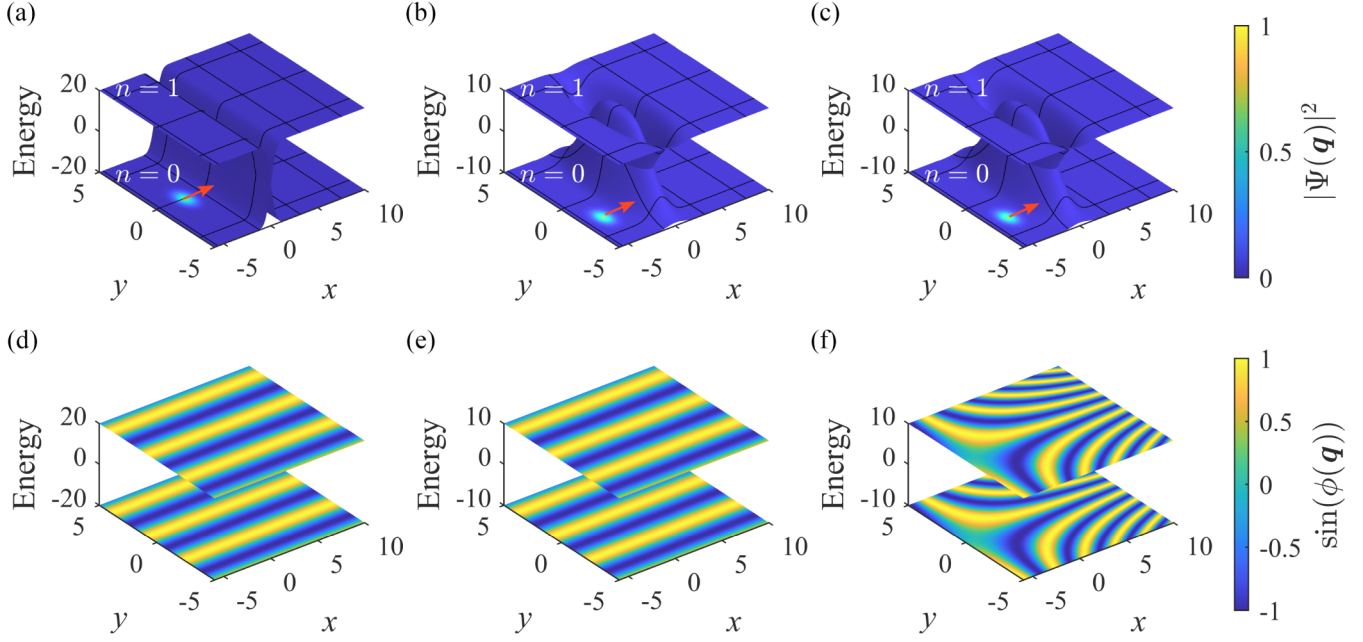
FIG. 1. Visualization of the (a)–(c) diabatic and (d)–(f) adiabatic surfaces for models (a) and (d) A, (b) and (e) B, and (c) and (f) C with parameters given in the text and $W = 2.0$. Superimposed on the diabatic surfaces are heat maps depicting the nuclear wave-packet intensity as initialized on the $n = 0$ diabatic surface. Red arrows depict the initial momentum. Superimposed on the adiabatic surfaces are heat maps of $\sin[\phi(\boldsymbol{q})]$, representing the complex oscillation of the eigenvectors resulting from geometric phase effects that gives rise to complex-valued derivative couplings.

geometric rotation is increased, which, as we show below, introduces inaccuracies.

In accordance with the $\mathfrak{D}_{\min}$ approach, one particular diabatic basis $D_{\bar{k}}$ which happens to minimize the metric involves the functional representation

$$\lambda = A, \quad R^{\bar{k}} = -\frac{\pi}{4}\mathrm{erf}(Bx), \quad I^{\bar{k}} = \frac{1}{2}Wy. \quad (10)$$

The associated metric is

$$\mathfrak{D}(I^{\bar{k}}) = \tfrac{1}{2}|W|, \quad (11)$$

with the rescaling direction governed by

$$\tilde{V}^{\dagger}(R^{\bar{k}})\nabla\tilde{V}(R^{\bar{k}}) = -\frac{\sqrt{\pi}}{2}Be^{-B^2x^2}\hat{x}T^R, \quad (12)$$

where $\hat{x}$ denotes the unit vector in the x direction and T^R is the real-valued off-diagonal generator of SU(2) provided in Appendix B. From the survey presented in the SM [42], it follows that Eq. (11) is a minimum shared by a set of preferred bases that extends beyond $\bar{k}$, all yielding the same momentum rescaling direction up to an overall sign. Hence, $\mathfrak{D}_{\min}$ predicts that momentum should be unambiguously rescaled in the x direction upon a nonadiabatic transition.

In what follows, we will compare results from FSSH within $\mathfrak{D}_{\min}$ to those obtained within $\mathfrak{R}_{\max}$ and against exact quantum results obtained with the Fourier transform method [43]. In doing so, we consider $W = 0.0$, $W = 2.0$, and $W = 3.0$ while fixing $A = 20$ and $B = 1.0$. The nuclear wave packet is initialized on a single diabatic surface [44] as

$$\Psi(\boldsymbol{q}) = e^{i\boldsymbol{q}\cdot\boldsymbol{p}_{\mathrm{init}}}e^{-|\boldsymbol{q}-\boldsymbol{q}_{\mathrm{init}}|^2} \quad (13)$$

while being centered at $\boldsymbol{q}_{\mathrm{init}} = (-3, 0)$ and while moving towards the avoided crossing with $\boldsymbol{p}_{\mathrm{init}} = (p^x_{\mathrm{init}}, 0)$, as depicted in Fig. 1. Meanwhile, p^x_{init} is varied between 8 and 24. Since the diabatic surfaces cross but the adiabatic surfaces do not, a fully adiabatic trajectory (with no hops) yields transmitted populations fully on the opposite diabatic surface.

Figure 2 shows results with the nuclear wave packet initialized on the $n = 0$ diabatic surface, which initially corresponds to the diabatic surface at the lowest energy. This roughly corresponds to an initialization on the lower adiabatic surface, as the diabatic and adiabatic surfaces coincide at the initial wave-packet location (see Fig. 1). Such an initialization is particularly interesting, as virtually all nonadiabatic transitions require energy to be absorbed from the momentum within FSSH. With $\mathfrak{D}_{\min}$ predicting $\hat{x}$ rescaling, the rate of nonadiabatic transitions is thus sensitively dependent on the value of p^x_{init}. Hence, comparing transient populations against exact quantum results makes for a sensitive test case for the $\hat{x}$ rescaling prediction. Results with an initialization on the other ($n = 1$) diabatic surface (for which the nonadiabatic transitions are less trivially related to momentum rescaling) are included in the SM [42], and animations of the full wavepacket dynamics for $p^x_{\mathrm{init}} = 24$ and $W = 3.0$ are also provided there.

For $W = 0.0$, meaning in the absence of geometric phase effects, both $\mathfrak{D}_{\min}$ and $\mathfrak{R}_{\max}$ yield the same rescaling direction within FSSH, corresponding to the direction in which momenta are conventionally rescaled within topologically trivial systems. This is borne out in Fig. 2, where both approaches are seen to produce identical results, which are in near-quantitative agreement with exact results save for small deviations inherent to FSSH. $\mathfrak{D}_{\min}$ retains a consistent perfor-
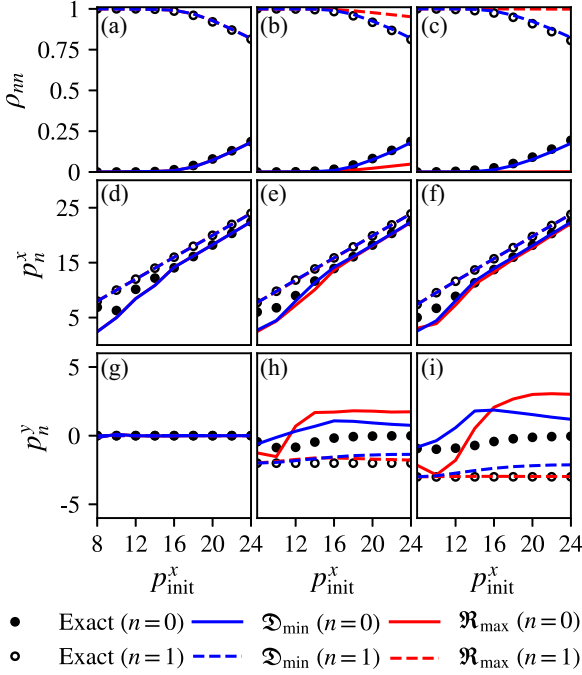
FIG. 2. Calculated results for a nuclear wave packet traversing an avoided-crossing region described by model A [Eq. (9)] with (a), (d), and (g) $W = 0.0$, (b), (e), and (h) $W = 2.0$, and (c), (f), and (i) $W = 3.0$. Results from FSSH under application of the $\mathfrak{D}_{\min}$ approach are compared with exact results and with those from FSSH under application of the $\mathfrak{R}_{\max}$ approach [35]. Shown are the transmitted population ρ_{nn} and the x and y components of momentum (p_n^x and p_n^y, respectively) for the $n = 1$ and $n = 0$ diabatic surfaces. The nuclear wave packet is initialized on the $n = 0$ diabatic surface.

mance throughout all values of W, again within the limitations imposed by FSSH. In particular, the transmitted populations ρ_{nn} show quantitative agreement with exact results across the full range of initial momenta, underscoring the validity of exclusive $\hat{x}$ rescaling. The latter is further substantiated by the high accuracy reached for the x component of the transmitted momenta p_n^x for both diabatic surfaces. Trajectories that remain on the same adiabatic surface arrive on the $n = 1$ diabatic surface with $p_1^x \approx p_{\text{init}}^x$ as expected. The trajectories that arrive on the $n = 0$ diabatic surface, however, lose momentum due to $\hat{x}$ rescaling that occurs following a hop.

According to $\mathfrak{D}_{\min}$, the y component of the transmitted momentum is affected only by pseudomagnetic forces. This prediction is consistent with results for p_n^y shown in Fig. 2, where moderate deviations from the exact result can be attributed to a breakdown of the FSSH algorithm in the presence of such forces. For example, the overestimation of p_1^y is due to trajectories hopping twice in the crossing region (therefore arriving on $n = 1$) and experiencing the opposite pseudomagnetic force on the other adiabatic surface, reducing the net transmitted momentum from the expected result of $p_1^y = -W$ (which was derived analytically in Ref. [35]).

Similarly, p_0^y is overestimated due to the randomized location of the hops in the crossing region. In the SM [42], we demonstrate that these sources of inaccuracy can be controlled by confining hops to either the $x > 0$ or $x < 0$ region, yielding an underestimation and overestimation of p_0^y, respectively. (In

both cases, p_1^y shows a slightly improved agreement with exact results due to the reduced number of trajectories that hop twice, confirming that the observed inaccuracies are indeed due to a breakdown of FSSH in the presence of pseudomagnetic fields.) Notably, if the hops were constrained to the $x = 0$ point the trajectories would arrive with exactly $p_0^y = 0$, having experienced the opposite pseudomagnetic forces on both surfaces and thereby acquiring no net momentum in the y direction. As such, the surface-hopping technique proposed by Tully and Preston [8], in which hops occur only at avoided crossings, would predict values of $p_0^y = 0$, in better agreement with exact results [35].

For $\mathfrak{R}_{\max}$, on the other hand, we find qualitative differences from exact results to be much more pronounced. For the applied parameters, this approach predicts $\hat{y}$ rescaling when $|x| \leqslant 0.48$ ($|x| \leqslant 1.21$) for $W = 2.0$ ($W = 3.0$) and $\hat{x}$ rescaling otherwise. Hence, rescalings along the y direction occur particularly close to the crossing region. As a consequence, the lack of initial momentum in this direction inhibits the rate of upward transitions from the lower to upper adiabatic surface. This is borne out in Fig. 2, where $\mathfrak{R}_{\max}$ is seen to significantly underestimate population transfer. Concomitantly, significant deviations are found for p_0^y. Interestingly, p_1^y incidentally agrees with exact results because $\hat{y}$ rescaling prevents trajectories from hopping twice due to insufficient momentum. Overall, however, the deviations introduced by $\mathfrak{R}_{\max}$ lead to qualitatively incorrect dynamics of the wave packet not seen for $\mathfrak{D}_{\min}$.

B. Models B and C

The second and third models, referred to as model B and model C, respectively, involve a rescaling direction that is dependent on the instantaneous position. Model B uses the same parametrization for ρ and ϕ as model A while modifying θ such that it has a gradient $\nabla\theta$ with a position-dependent direction,

$$\rho = A, \quad \theta = -\pi e^{-\frac{1}{3}(B_x x^2 + B_y y^2)}, \quad \phi = Wy. \quad (14)$$

Model C builds on model B, while parametrizing ϕ such that its gradient also has a position-dependent direction,

$$\rho = A, \quad \theta = -\pi e^{-\frac{1}{3}(B_x x^2 + B_y y^2)}, \quad \phi = W\left(y + \frac{1}{5}xy\right). \quad (15)$$

Like model A, the Hamiltonians produced under models B and C are topologically trivial for $W = 0.0$ and become increasingly nontrivial for larger values of W. Unlike model A, models B and C feature *two* diabatic crossings, so a trajectory that does not switch adiabatic surfaces finds itself on the same diabatic surface outside of the crossing region, as shown in Fig. 1. From the survey of the metric and rescaling direction, presented in the SM [42], it follows that, different from the $\hat{x}$ rescaling found for model A, models B and C involve $\nabla\theta$ rescaling whose direction depends on the position.

In the following, we again compare results from FSSH within $\mathfrak{D}_{\min}$ to those obtained within $\mathfrak{R}_{\max}$. We take $A = 10$, $B_x = 1.00$, and $B_y = 0.25$ for both models B and C while initializing the nuclear wave packet like in model A, but with $\mathbf{q}_{\text{init}} = (-4, -2)$. Figures 3 and 4 show results for models B and C, respectively, with the nuclear wave packet initialized on the $n = 0$ diabatic surface. As before, the SM [42] includes
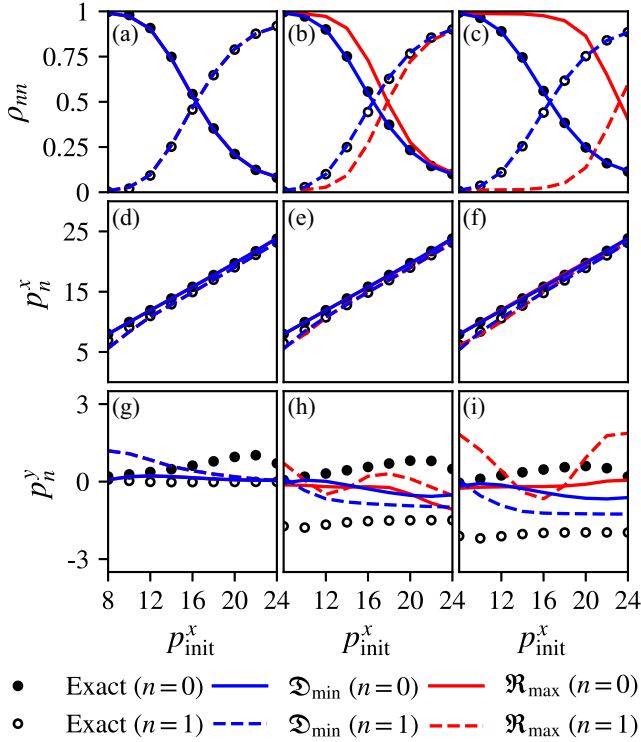
FIG. 3. Same as Fig. 2, but for model B [Eq. (14)] with (a), (d), and (g) $W = 0.0$, (b), (e), and (h) $W = 1.5$, and (c), (f), and (i) $W = 2.0$.
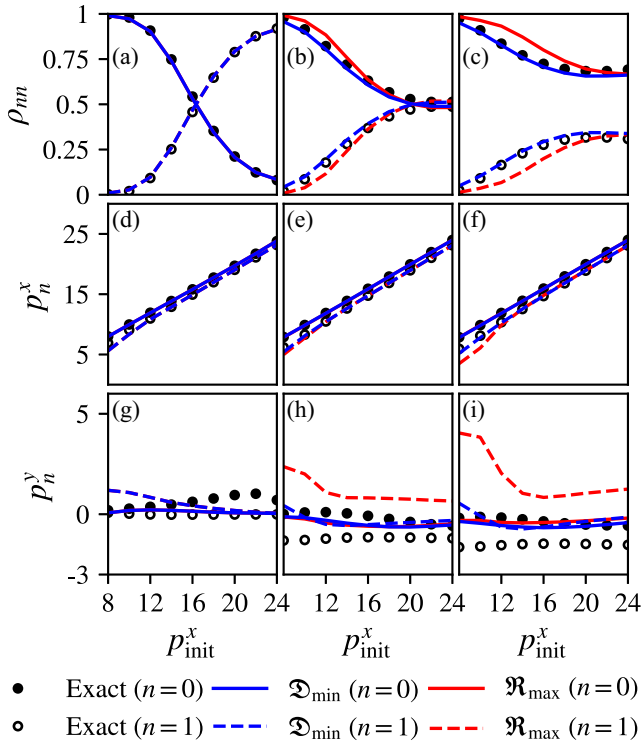
FIG. 4. Same as Fig. 2, but for model C [Eq. (15)] with (a), (d), and (g) $W = 0.0$, (b), (e), and (h) $W = 1.5$, and (c), (f), and (i) $W = 2.0$.

results with initialization on the $n = 1$ diabatic surface, and animations of the full wave-packet dynamics for $p_{\mathrm{init}}^x = 24$ and $W = 2.0$ are also provided there.

Notably, both models B and C involve deviations in p_n^y even for $W = 0.0$, which reflects inherent inadequacies of FSSH in treating these models in the absence of geometric phase effects. When geometric phase effects are turned on by taking $W = 1.5$ or $W = 2.0$, deviations in p_n^y grow appreciably for both $\mathfrak{D}_{\mathrm{min}}$ and $\mathfrak{R}_{\mathrm{max}}$, although the former retains a well-behaved trend overall, and its deviations from exact results are less pronounced, especially for p_1^y. As for model A, it is plausible that these deviations are attributable to shortcomings of the FSSH algorithm in the presence of pseudomagnetic fields, rather than the $\mathfrak{D}_{\mathrm{min}}$ approach, although it is challenging to assess this as we did for model A due to the nontrivial dependence of the momentum rescaling direction on the position for models B and C. Nonetheless, this attribution is consistent with calculated values of ρ_{nn}, for which $\mathfrak{D}_{\mathrm{min}}$ is once more seen to reach quantitative accuracy. For $\mathfrak{R}_{\mathrm{max}}$ significant deviations are observed for this quantity. Both rescaling approaches generally perform well for p_n^x.

IV. CONCLUSION AND OUTLOOK

To conclude, our bottom-up construction of parametric Hamiltonians establishes a continuity between topologically trivial and topologically nontrivial systems, resolving a conceptual discontinuity in how such systems have previously been treated in trajectory surface hopping methods. By defining a functional representation, the gauge ambiguity arising for topologically nontrivial systems is brought on equal footing with that of the topologically trivial case. This provides a framework by which the gauge freedom of the derivative couplings can be restricted, even in the presence of geometric phase effects, and momentum rescaling directions can be determined within trajectory surface hopping techniques.

The resulting approach, $\mathfrak{D}_{\mathrm{min}}$, produces FSSH results in favorable agreement with exact quantum modeling and offers a general improvement over a previously proposed rescaling approach [35], here referred to as $\mathfrak{R}_{\mathrm{max}}$. Notably, while $\mathfrak{R}_{\mathrm{max}}$ was found to disagree with exact results for the parameters used here, it was previously shown to yield good agreement with exact results for model A under a wide range of parameter choices [35]. Notably, for all of these cases $\mathfrak{R}_{\mathrm{max}}$ predicts a momentum rescaling along $\hat{x}$. As such, the $\mathfrak{D}_{\mathrm{min}}$ approach introduced in this article emerges as an equally viable means of momentum rescaling in these particular instances, but one that is more broadly generalizable.

In closing, we would like to share a perspective on the application of our approach beyond the two-dimensional avoided crossings explored in the present work. Notably, establishing the functions for a given Hamiltonian can be done numerically by using a grid of $\boldsymbol{q}$ points, avoiding the need for deriving their analytic expressions. In the SM [42], we present a proof of concept of a fully numerical evaluation of the functions and resulting metrics for model A, where it is noted that the sum in Eq. (6) fortuitously is prone to truncating at finite order and that minimizing the metric can, in principle, be performed iteratively, similarly to how a molecular geometry optimization is performed. Such fully numerical

evaluations open potential opportunities for the application of our approach to *ab initio* trajectories, which additionally requires the use of a diabatization scheme [45–52].

Although applications of our approach to high-dimensional systems may generally pose a challenge, an interesting exception is formed by simple lattice models, which provide a popular route for studying the fundamental physics of topological materials [53] and for which our approach can be readily applied by virtue of them being analytically parametrized in a well-defined diabatic basis. Hence, our present work is of particular relevance to emergent efforts applying trajectory surface hopping techniques to lattice models. It is noteworthy that our approach is fully consistent with our previous study [54], which found that truncated reciprocal-space lattice Hamiltonians may yield complex-valued derivative couplings. In this case, a truncated discrete Fourier transform can be applied to bring the system into a preferred basis in order to find real-valued derivative couplings. This reflects the lack of geometric phase effects in the equivalent real-space Hamiltonian [55]. In addition to lattice models, it is conceivable that other classes of problems provide similar analytical routes through which our approach can be applied readily.

APPENDIX A: CONSTRUCTION OF *V* FROM THE GENERATORS OF SU(*N*)

In its most general form an eigenvector matrix V_0 is an element of U(*N*) by virtue of its unitarity. By the multiplicativity of the determinant, V_0 can be made into an element of SU(*N*) through a gauge transformation that leaves H_0 unchanged. It therefore suffices to construct a generic eigenvector matrix V

as an element of SU(*N*), i.e.,

$$V(\boldsymbol{I}, \boldsymbol{R}, \boldsymbol{G}) = \prod_{n_i} \exp\left(I_{n_i} T_{n_i}^I\right) \prod_{n_r} \exp\left(R_{n_r} T_{n_r}^R\right)$$
$$\times \prod_{n_e} \exp\left(G_{n_e} T_{n_e}^E\right), \tag{A1}$$

where $\boldsymbol{I} = (I_1, I_2, \ldots, I_{N'})$, $\boldsymbol{R} = (R_1, R_2, \ldots, R_{N'})$, and $\boldsymbol{G} = (G_1, G_2, \ldots, G_{N-1})$ are functions associated with the subsets $\{T_{n_i}^I\}$, $\{T_{n_r}^R\}$, and $\{T_{n_e}^E\}$, respectively.

The ordering of generators in Eq. (A1) is taken as a convention, and the inclusion of the terms associated with $\{T_{n_e}^E\}$ in Eq. (A1) is an intentional one meant to emphasize their role as gauge transformations. Variations in $\boldsymbol{G}$ leave the Hamiltonian unchanged, so these terms can be discarded. Therefore, instead of SU(*N*) we represent V by a subset of SU(*N*) which still accounts for every possible Hamiltonian, leading to Eq. (2).

APPENDIX B: CONSTRUCTION OF *H* FROM THE GENERATORS OF SU(2)

For $N = 2$, H can be constructed by employing the generators of SU(2), given by

$$T^E = \begin{pmatrix} i & 0 \\ 0 & -i \end{pmatrix}, \quad T^R = \begin{pmatrix} 0 & -1 \\ 1 & 0 \end{pmatrix}, \quad T^I = \begin{pmatrix} 0 & i \\ i & 0 \end{pmatrix}. \tag{B1}$$

A generic eigenvector matrix can be written following Eq. (2),

$$V(I, R) = \exp(IT^I) \exp(RT^R). \tag{B2}$$

The eigenvalue matrix, on the other hand, follows from Eq. (1),

$$E(\lambda) = \begin{pmatrix} -\lambda & 0 \\ 0 & \lambda \end{pmatrix}, \tag{B3}$$

upon which the Hamiltonian follows from Eq. (3) as

$$H(\lambda, I, R) = V(I, R)E(\lambda)V^\dagger(I, R)$$
$$= \lambda \begin{pmatrix} -\cos(2R)\cos(2I) & -\sin(2R) + i\cos(2R)\sin(2I) \\ -\sin(2R) - i\cos(2R)\sin(2I) & \cos(2R)\cos(2I) \end{pmatrix}. \tag{B4}$$

APPENDIX C: DERIVATION OF CLASSICAL EQUATIONS OF MOTION

Trajectory surface hopping techniques assume adiabatic evolution of a quantum state on a single adiabatic surface in between hops, denoted by α. This corresponds to the Born-Huang approximation under which the classical Hamiltonian takes the form [6]

$$H^{\text{cl}} = \tfrac{1}{2}(\tilde{\boldsymbol{p}} - \boldsymbol{A}_\alpha)^2 + V_\alpha(\boldsymbol{q}). \tag{C1}$$

Here, $\tilde{\boldsymbol{p}}$ is the gauge-dependent canonical momentum, and $\boldsymbol{A}_\alpha \equiv i\langle\alpha|\nabla\alpha\rangle$ is the gauge potential. Classical mechanics involves the kinetic momentum $\boldsymbol{p} = \tilde{\boldsymbol{p}} - \boldsymbol{A}_\alpha = \dot{\boldsymbol{q}}$, where the second equality assumes all classical masses are set to unity. Note that in the main text it is the kinetic momenta that are

sampled to represent the nuclear wave packet and the canonical momenta are never explicitly utilized. This approach is consistent with how FSSH is ordinarily applied, seeing that for topologically trivial systems the difference between the kinetic and canonical momenta vanishes in the appropriate gauge.

The equations of motion then follow as

$$\dot{q}_\nu = \frac{\partial H^{\text{cl}}}{\partial p_\nu} \tag{C2}$$

and

$$\dot{p}_\nu = -\frac{\partial H^{\text{cl}}}{\partial q_\nu} - \frac{dA_\alpha^\nu}{dt}$$

$$= \sum_{\mu} \left(\tilde{p}_{\mu} - A_{\alpha}^{\mu} \right) \frac{\partial A_{\alpha}^{\mu}}{\partial q_{\nu}} - \frac{\partial A_{\alpha}^{\nu}}{\partial q_{\mu}} \dot{q}_{\mu} - \frac{\partial V_{\alpha}}{\partial q_{\nu}}$$

$$= \sum_{\mu} p_{\mu} \left(\frac{\partial A_{\alpha}^{\mu}}{\partial q_{\nu}} - \frac{\partial A_{\alpha}^{\nu}}{\partial q_{\mu}} \right) - \frac{\partial V_{\alpha}}{\partial q_{\nu}}, \qquad \text{(C3)}$$

where we made use of the chain rule to obtain the gauge-invariant pseudomagnetic force terms, which are reminiscent of the Lorentz force on a charged particle in a magnetic field.

[1] M. V. Berry, Proc. R. Soc. London, Ser. A **392**, 45 (1984).

[2] M. Baer, *Beyond Born-Oppenheimer: Conical Intersections and Electronic Nonadiabatic Coupling Terms* (Wiley, Hoboken, NJ, 2006).

[3] S. K. Min, A. Abedi, K. S. Kim, and E. K. U. Gross, Phys. Rev. Lett. **113**, 263004 (2014).

[4] V. Krishna, J. Chem. Phys. **126**, 134107 (2007).

[5] J. Subotnik, G. Miao, N. Bellonzi, H.-H. Teh, and W. Dou, J. Chem. Phys. **151**, 074113 (2019).

[6] C. A. Mead, Rev. Mod. Phys. **64**, 51 (1992).

[7] We make a point of referring to only topologically nontrivial systems as having geometric phase effects despite the fact that nonadiabatic dynamics in topologically trivial systems can also be considered as a type of geometric rotation [56].

[8] J. C. Tully and R. K. Preston, J. Chem. Phys. **55**, 562 (1971).

[9] J. C. Tully, Int. J. Quantum Chem. **40**, 299 (1991).

[10] M. Barbatti, Wiley Interdiscip. Rev.: Comput. Mol. Sci. **1**, 620 (2011).

[11] L. Yu, C. Xu, Y. Lei, C. Zhu, and Z. Wen, Phys. Chem. Chem. Phys. **16**, 25883 (2014).

[12] J. C. Tully, J. Chem. Phys. **93**, 1061 (1990).

[13] S. Hammes-Schiffer and J. C. Tully, J. Chem. Phys. **101**, 4657 (1994).

[14] X. Bian, Y. Wu, H.-H. Teh, Z. Zhou, H.-T. Chen, and J. E. Subotnik, J. Chem. Phys. **154**, 110901 (2021).

[15] Y. Wu, X. Bian, J. I. Rawlinson, R. G. Littlejohn, and J. E. Subotnik, J. Chem. Phys. **157**, 011101 (2022).

[16] W. Xie and W. Domcke, J. Chem. Phys. **147**, 184114 (2017).

[17] X. Bian, Y. Wu, H.-H. Teh, and J. E. Subotnik, J. Chem. Theory Comput. **18**, 2075 (2022).

[18] S. Mai, P. Marquetand, and L. González, Int. J. Quantum Chem. **115**, 1215 (2015).

[19] Y. Wu, G. Miao, and J. E. Subotnik, J. Phys. Chem. A **124**, 7355 (2020).

[20] Y. Wu and J. E. Subotnik, Nat. Commun. **12**, 700 (2021).

[21] B. Göhler, V. Hamelbeck, T. Z. Markus, M. Kettner, G. F. Hanne, Z. Vager, R. Naaman, and H. Zacharias, Science **331**, 894 (2011).

[22] R. Naaman and D. H. Waldeck, J. Phys. Chem. Lett. **3**, 2178 (2012).

[23] R. Naaman and D. H. Waldeck, Annu. Rev. Phys. Chem. **66**, 263 (2015).

[24] R. Naaman, Y. Paltiel, and D. H. Waldeck, Nat. Rev. Chem. **3**, 250 (2019).

[25] C. Xie, D. R. Yarkony, and H. Guo, Phys. Rev. A **95**, 022104 (2017).

[26] C. Xie, C. L. Malbon, H. Guo, and D. R. Yarkony, Acc. Chem. Res. **52**, 501 (2019).

[27] D. Yuan, Y. Huang, W. Chen, H. Zhao, S. Yu, C. Luo, Y. Tan, S. Wang, X. Wang, Z. Sun, and X. Yang, Nat. Commun. **11**, 3640 (2020).

[28] D. A. Fedorov, S. R. Pruitt, K. Keipert, M. S. Gordon, and S. A. Varganov, J. Phys. Chem. A **120**, 2911 (2016).

[29] A. Hauser, A. Vef, and P. Adler, J. Chem. Phys. **95**, 8710 (1991).

[30] M. Richter, S. Mai, P. Marquetand, and L. González, Phys. Chem. Chem. Phys. **16**, 24423 (2014).

[31] Z. Nie, R. Long, L. Sun, C.-C. Huang, J. Zhang, Q. Xiong, D. W. Hewak, Z. Shen, O. V. Prezhdo, and Z.-H. Loh, ACS Nano **8**, 10931 (2014).

[32] Y. Shi, O. V. Prezhdo, J. Zhao, and W. A. Saidi, ACS Energy Lett. **5**, 1346 (2020).

[33] B. Datta, P. C. Adak, L.-k. Shi, K. Watanabe, T. Taniguchi, J. C. W. Song, and M. M. Deshmukh, Sci. Adv. **5**, eaax6550 (2019).

[34] X. Bian, Y. Wu, J. Rawlinson, R. G. Littlejohn, and J. E. Subotnik, J. Phys. Chem. Lett. **13**, 7398 (2022).

[35] G. Miao, N. Bellonzi, and J. Subotnik, J. Chem. Phys. **150**, 124101 (2019).

[36] Y. Wu and J. E. Subotnik, J. Chem. Phys. **154**, 234101 (2021).

[37] P. Pechukas, Phys. Rev. **181**, 166 (1969).

[38] P. Pechukas, Phys. Rev. **181**, 174 (1969).

[39] An example is the case where the real-valued eigenvectors $|\alpha\rangle$ and $|\beta\rangle$ are transformed as $|\alpha'\rangle = |\alpha\rangle$ and $|\beta'\rangle = e^{i\frac{\pi}{2}}|\beta\rangle$, yielding the fully imaginary-valued derivative coupling $\langle\alpha'|\nabla\beta'\rangle$.

[40] Here we implicitly assume an eigendecomposition in which real-valued Hamiltonians always give rise to real-valued eigenvectors, but complex-valued Hamiltonians under the same convention give rise to complex-valued eigenvectors.

[41] Because the equation $H(\boldsymbol{\lambda}(\boldsymbol{q}), \boldsymbol{I}(\boldsymbol{q}), \boldsymbol{R}(\boldsymbol{q})) = H_0(\boldsymbol{q})$ may have multiple solutions, we refer to properties of the entire set of solutions when requiring that $\nabla\boldsymbol{I} \neq 0$, such that if even one solution has $\nabla\boldsymbol{I} = 0$, Eq. (4) becomes real valued.

[42] See Supplemental Material at http://link.aps.org/supplemental/10.1103/PhysRevA.109.032210 for a survey of diabatic bases, FSSH results for $n = 1$ diabatic surface initialization, a numerical evaluation of the functions, a demonstration of the influence of stochastic hops on p_n^y, and animations of the full wave-packet dynamics.

[43] D. Kosloff and R. Kosloff, J. Comput. Phys. **52**, 35 (1983).

[44] FSSH trajectories are initialized by sampling both adiabatic surfaces to stochastically reproduce the initial diabatic populations.

[45] J. E. Subotnik, S. Yeganeh, R. J. Cave, and M. A. Ratner, J. Chem. Phys. **129**, 244101 (2008).

[46] J. E. Subotnik, E. C. Alguire, Q. Ou, B. R. Landry, and S. Fatehi, Acc. Chem. Res. **48**, 1340 (2015).

[47] M. Baer, Chem. Phys. **15**, 49 (1976).

[48] C. A. Mead and D. G. Truhlar, J. Chem. Phys. **77**, 6090 (1982).

[49] T. Van Voorhis, T. Kowalczyk, B. Kaduk, L.-P. Wang, C.-L. Cheng, and Q. Wu, Annu. Rev. Phys. Chem. **61**, 149 (2010).

[50] H. Guo and D. R. Yarkony, Phys. Chem. Chem. Phys. **18**, 26335 (2016).

[51] H.-J. Werner and W. Meyer, J. Chem. Phys. **74**, 5802 (1981).

[52] C. E. Hoyer, K. Parker, L. Gagliardi, and D. G. Truhlar, J. Chem. Phys. **144**, 194101 (2016).

[53] K. Sun, Z. Gu, H. Katsura, and S. Das Sarma, Phys. Rev. Lett. **106**, 236803 (2011).

[54] A. Krotz and R. Tempelaar, J. Chem. Phys. **156**, 024105 (2022).

[55] A. Krotz, J. Provazza, and R. Tempelaar, J. Chem. Phys. **154**, 224101 (2021).

[56] J. Anandan, Phys. Lett. A **133**, 171 (1988).